47th AIAA Aerospace Sciences Meeting Including The New Horizons Forum and Aerospace Exposition
5 - 8 January 2009, Orlando, Florida

AIAA 2009-271

Aerodynamic and Aeroacoustic Properties of a Flatback Airfoil: An Update

Matthew F. Barone*, Dale Berg†
Sandia National Laboratories
Albuquerque, NM 87185

Results from an experimental study of the aerodynamic and aeroacoustic properties of a flatback version of the TU Delft DU97-W-300 airfoil are presented for a chord Reynolds number of 3×10^6. The data were gathered in the Virginia Tech Stability Wind Tunnel, which uses a special aeroacoustic test section to enable measurements of airfoil self-noise. Corrected wind tunnel aerodynamic measurements for the DU97-W-300 are compared to previous solid wall wind tunnel data and are shown to give good agreement. Aeroacoustic data are presented for the flatback airfoil, with a focus on the amplitude and frequency of noise associated with the vortex-shedding tone from the blunt trailing edge wake. The effect of a splitter plate attachment on both drag and noise is also presented. Computational Fluid Dynamics predictions of the aerodynamic properties of both the unmodified DU97-W-300 and the flatback version are compared to the experimental data.

I. Introduction

Design of the inboard region of wind turbine blades involves a compromise between aerodynamic performance, structural requirements and, at large scale, size constraints due to considerations such as land transportation of blades. The flatback airfoil concept was motivated by these multi-disciplinary considerations. The shape of a flatback airfoil is generated by taking an existing airfoil shape and adding thickness about the camber line over some aft portion of the airfoil, resulting in an airfoil with the same camber line as the original, but with a blunt base at the trailing edge. This approach is in contrast to "truncated" airfoils where the trailing edge is simply cut off, changing the camber and degrading airfoil lift performance. The primary structural advantage of the flatback shape is that its sectional strength is larger than that of a sharp trailing edge airfoil for a given chord length. This property can be leveraged to decrease blade weight and cost, both critical issues for the next generation of wind turbine blades.[1] Aerodynamic benefits include increased lift curve slope, increased maximum lift, and reduced sensitivity to stall caused by leading edge soiling.[2]

Technical risks associated with the use of flatback airfoils for the inboard region of wind turbine blades include increased aerodynamic noise and increased aerodynamic drag. Both of these penalties are the result of the blunt trailing edge shape and the wake that is produced by this shape. The relatively low pressure at the blunt base results in a much larger drag force than for a conventional airfoil shape. The effect of this drag penalty on rotor thrust and torque coefficient for typical inboard twist angles is not severe, and in fact can be offset by the additional lift that a flatback airfoil generates.[3] Consideration of drag reducing devices such as splitter plates or trailing edge serrations may be desireable to further boost performance, however.

The increased noise from the flatback is due primarily to the vortex shedding phenomenon associated with bluff-body wakes. The vortex shedding often leads to tonal noise, similar to the Aeolian tones of flow past circular cylinders. The intensity of bluff-body vortex shedding tones at low Mach number scales with the sixth power of the relative flow velocity. Broadband aeroacoustic noise sources associated with turbulent boundary layer-trailing edge interaction scale with the fifth power of the relative flow velocity. Since outboard flow velocities are much higher than those encountered inboard, the overall aerodynamic noise levels of a rotor incorporating inboard flatback shapes will likely continue to be dominated by outboard trailing edge noise. However, two aspects of the flatback noise source may be cause for concern. First, the vortex-shedding noise from flatbacks is likely to be contained in a relatively low-frequency band (50-200 Hz). Some community noise regulations have separate low-frequency noise standards apart from consideration of A-weighted sound, which emphasize higher frequencies to which the human ear is more sensitive. Second, the

*Wind Energy Technology Department., MS 1124, mbarone@sandia.gov
†Wind Energy Technology Department., MS 1124

source of the flatback noise is likely to be tonal in nature. Pure tones are perceived as more annoying than broadband noise, often resulting in special treatment of tones in noise standards.

Previous work on analysis and testing of flatback airfoils includes wind tunnel testing at moderate Reynolds numbers,[2] as well as computational modeling of flatback airfoils and their effect on rotor performance.[3,4] The goals of the present study are: 1) measure aerodynamic performance of flatback airfoils at higher Reynolds numbers representative of those encountered by utility scale wind turbines, including quantification of the drag penalty 2) quantify the aeroacoustic noise from a flatback airfoil, 3) assess the effect of a simple splitter plate attachment on flatback drag and noise, and 4) validate computational models of flatback aerodynamics and aeroacoustics against experimental data. To this end, a wind tunnel experiment was performed to measure the aerodynamic and aeroacoustic characteristics of the TU-Delft DU97-W-300 airfoil[5] and a flatback version of that airfoil, the DU97-flatback (see Figure 1). The DU97-flatback was created by adding thickness to the aft half of the airfoil, giving a blunt trailing edge with a width of 10% chord. An initial description of the experimental effort can be found in Berg and Zayas.[6] The present paper provides an update on the experimental effort and presents computational results for prediction of flatback aerodynamics. A separate paper[7] describes efforts to model the flatback aeroacoustics using numerical simulation of the unsteady flatback wake.

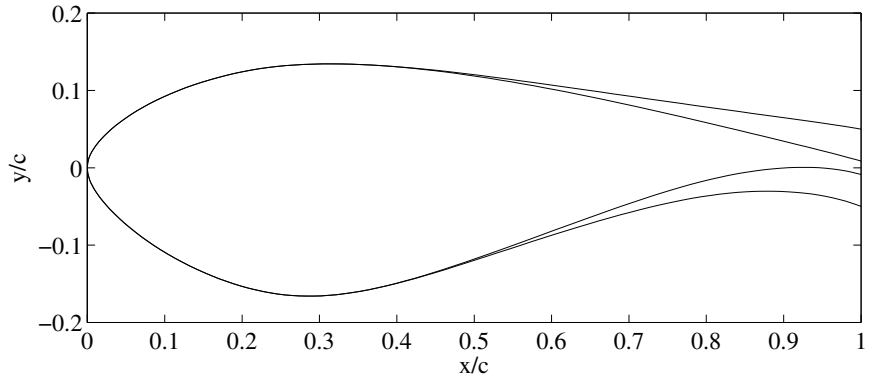

Figure 1. DU97-W-300 and DU97-flatback airfoils.

II. Experiment: Facilities and Instrumentation

The experimental measurements were obtained in the Virginia Tech Stability Wind Tunnel, a closed-loop subsonic wind tunnel with a 1.83 meter square test section. This tunnel has a removable solid wall test section that can be replaced with an aeroacoustic test section suitable for making measurements of airfoil self-noise. The aeroacoustic test section incorporates sound-absorbing panels in the upper and lower test section walls (the airfoil is mounted vertically to these walls), while the side walls are constructed from Kevlar material that allows sound to exit the test section without reflection or attenuation. The Kevlar also largely confines the flow, although it is a porous material that allows a small amount of mass flow across the tunnel walls. The walls of the side chambers surrounding the test section are treated with anechoic foam wedges that effectively absorb sound with frequencies above approximately 140 Hz. More details of this facility can be found in Remillieux *et al.*[8]

As described in Berg and Zayas,[6] aerodynamic forces, moments, and surface pressure profiles were measured for the DU97-W-300, the DU97-flatback, and the DU97-flatback fitted with a splitter plate attachment on the airfoil base. The splitter plate was fashioned from an L-shaped aluminum bracket. It had a length equal to the base height, a thickness of 4.8 mm, and extended from the center of the airfoil base. Lift and moment coefficients were obtained by integration of surface pressure profiles, while drag was measured using a pitot-tube survey of the wake. These measurements were performed for a limited number of angles of attack and at several chord Reynolds numbers ranging from 1.6×10^6 to 3.2×10^6. Unless otherwise noted, all of the data presented herein are for $Re_c = 3.0 - 3.2 \times 10^6$ and with free boundary layer transition (no trip). Aeroacoustic measurements were made using a microphone array and a beamforming technique to isolate trailing edge noise sources above 500 Hz. For frequencies below 500 Hz, which included the measured flatback vortex shedding noise frequencies, spectra were computed by averaging the spectra from all of the microphones in the array.

III. Aerodynamic Wind Tunnel Data and Corrections

The aerodynamic testing of these airfoils in the aeroacoustic test section provided some unique challenges. Firstly, the relatively large model size and profile thickness introduced a significant solid blockage effect. Secondly, the lift interference and downwash corrections for the porous Kevlar walls had not been fully characterized for such thick airfoil models. This prompted follow-on testing to develop the appropriate wind tunnel wall corrections, including effects of mass flow through, as well as deflection of, the porous Kevlar walls. These corrections, currently under development, will be derived using an airfoil panel code with porous wall mass flow and wall deflection included to match free-boundary and in-tunnel pressure distributions. As part of this effort, the porosity of the Kevlar material was characterized by a static test. This test measured the velocity induced by a pressure difference across a sample of the Kevlar material stretched across a pipe entrance.

The empirical determination of the Kevlar wall porosity allows for some simple porous wall tunnel corrections to be applied as a surrogate for the more detailed corrections to come later. These corrections include: a solid blockage correction, modified by the porosity of the tunnel walls; a wake blockage correction; a lift interference "curvature" correction; and a downwash correction, induced by the porous walls. The approach is to apply the standard solid wall corrections of Allen and Vincenti,[9] then apply the solid blockage and downwash corrections for uniformly porous walls using "small model" porous wall corrections.[10] The assumptions in this simple correction method are that the velocity vs. pressure drop porosity relation is linear, that the Kevlar walls do not deflect, and that standard tunnel wall corrections may be accurately applied to flatback airfoils with thick, unsteady wakes. The first assumption is an approximation of the actual nonlinear relation between velocity and pressure drop across the porous wall, and the second assumption implies that the observed deflections of the Kevlar surface of 1-2 cm cause only small changes in the test section flow. The applicability of standard wind tunnel corrections to flatback airfoil testing was investigated by van Dam *et al.*[11] They determined that for the configurations considered (maximum airfoil thickness of 40% chord, maximum trailing edge width of 20% chord, and maximum solid blockage ratio of 10%), the standard corrections did perform well. The present solid blockage ratio is 15%, which introduces some uncertainty in application of the corrections. Due to these assumptions we conservatively estimate the uncertainty in the corrected lift and drag coefficients to be $\pm 5\%$, and the uncertainty in effective angle of attack to be ± 0.5 degrees. These uncertainties are reflected in the error bars included in all the plots of experimental data in this paper.

A measure of confidence in the present experimental results can be gained by comparison to a previous experiment of the DU97-W-300 performed in the TU-Delft low-speed, low-turbulence wind tunnel.[5] Data is available for a chord Reynolds number of 3×10^6 and a ratio of model chord to test section width of 0.33 (compared to 0.5 for the present experiments). The TU-Delft data is corrected for lift interference, solid wall blockage, and wake blockage using the method of Allen and Vincenti.[5,9] In Figure 2 and in Table 1, the TU-Delft data is compared to corrected measurements in the Virginia Tech tunnel with both solid wall and aeroacoustic (porous wall) test sections. Drag measurements were not made in the Virginia Tech solid wall test. Agreement in lift amongst the three tests is decent, while agreement in drag between the TU Delft and Virginia Tech tests is excellent. There is some disagreement in moment coefficient between the solid wall data and the Kevlar wall results.

Figure 3 compares pressure distributions, corrected for blockage, from the two facilities (solid-wall test section only) at effective angles of attack of 4 and 8 degrees. The two data sets agree extremely well with one another. The measured pressure distribution at angle of attack of 4 degrees for the aeroacoustic test section, not shown, deviates from the solid wall distributions by up to 10%, which may also help explain the discrepancy in moment coefficient. It is anticipated that the more detailed computational wall interference correction methods in progress will explain these differences.

Aerodynamic forces and moments for the DU97-flatback with and without the splitter plate are shown in Figure 4. The DU97-flatback has a higher lift curve slope and higher maximum lift coefficient than the DU97-W-300, in accordance with previous flatback airfoil studies. The nose-down pitching moment is greater for the flatback due to an increase in aft loading. The drag coefficient increases substantially for the flatback due to the blunt airfoil base. The splitter plate has the effect of slightly reducing the lift coefficient, decreasing the nose-down pitching moment, and decreasing the drag by approximately 45%. Note that the lift and moment coefficients for the DU97-flatback splitter plate were obtained from integrated surface pressure measurements and do not include the loads on the splitter plate itself. The reduction in drag from the splitter plate is similar to the reduction observed for different flatback airfoils at lower Reynolds numbers tested by Baker *et al.*[12]

Configuration	Geom. α	Eff. α	Meas. C_l	Corr. C_l	Meas. C_d	Corr. C_d	Meas. C_m	Corr. C_m
TU Delft Solid Wall	–	4.13	–	0.807	–	0.0112	–	−0.117
VA Tech Solid Wall	4.0	4.14	0.867	0.776	–	–	−0.129	−0.111
VA Tech Kevlar Wall	5.1	4.26	0.812	0.756	0.0112	0.0107	−0.142	−0.129
TU Delft Solid Wall	–	8.26	–	1.284	–	0.0132	–	−0.122
VA Tech Solid Wall	8.0	8.35	1.378	1.233	–	–	−0.139	−0.116
VA Tech Kevlar Wall	10.3	9.01	1.408	1.309	0.0149	0.0142	−0.165	−0.145

Table 1. Measured and corrected aerodynamic coefficients from wind tunnel data for the DU97-W-300, $\mathbf{Re_c = 3 \times 10^6}$.

Configuration	Geom. α	Eff. α	Meas. C_l	Corr. C_l	Meas. C_d	Corr. C_d	Meas. C_m	Corr. C_m
Flatback	5.1	4.12	0.908	0.833	0.0635	0.0598	−0.181	−0.164
Flatback	12.8	11.05	1.889	1.736	0.0578	0.0545	−0.230	−0.201
Flatback	15.4	13.40	2.207	2.033	0.0493	0.0466	−0.243	−0.210
Flatback w/ splitter	5.1	4.23	0.824	0.762	0.0345	0.0327	-0.155	-0.141
Flatback w/ splitter	12.8	11.14	1.814	1.679	0.0320	0.0304	-0.207	-0.181

Table 2. Measured and corrected aerodynamic coefficients from wind tunnel data for the DU97-flatback, $\mathbf{Re_c = 3 \times 10^6}$.

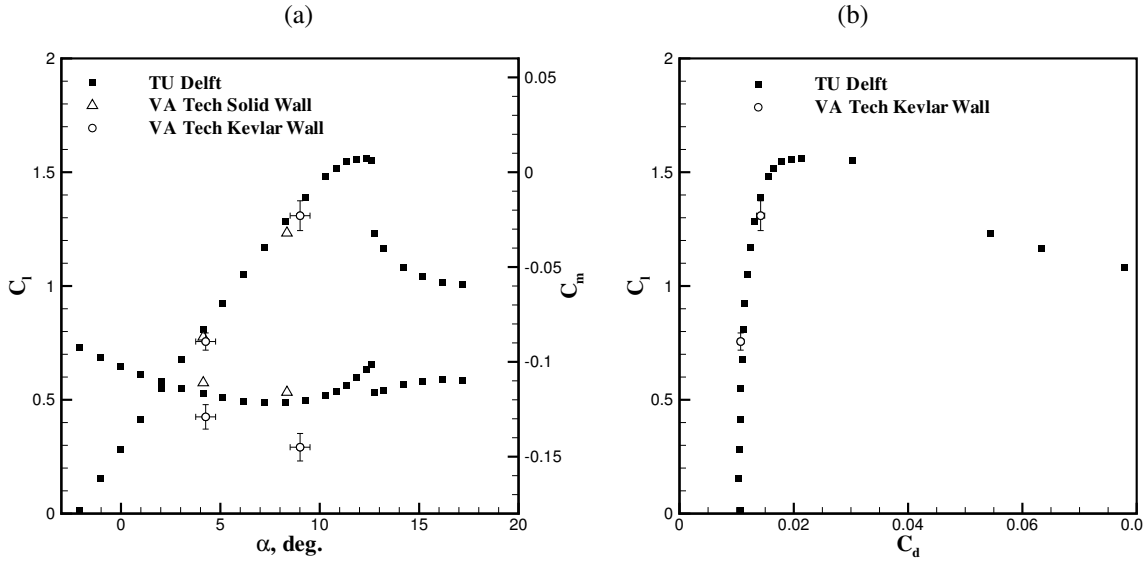

Figure 2. Measured lift, drag and moment coefficient for the DU97-W-300, $\mathbf{Re_c = 3 \times 10^6}$.

IV. Aeroacoustic Wind Tunnel Data and Corrections

Noise measurements of the DU97-W-300 and DU97-flatback with and without the splitter plate were made at a chord Reynolds number of $3.0 - 3.2 \times 10^6$. The tunnel free-stream velocity for these measurements was between 55.5 and 57.5 m/s. The center of the microphone array for all acoustic measurements was located in the symmetry plane of the airfoil model, at a distance 3.12 meters from the trailing edge and at an angle of 112 degrees from the streamwise (x) axis.

The aeroacoustic test section with anechoic wall treatment in the surrounding chamber is non-reflecting for sound frequencies above 200 Hz. Since the frequency of the vortex-shedding noise was between 140 and 200 Hz, the measurements of its amplitude required corrections to account for spurious reflections. This was accomplished by comparing the measured sound for a well-characterized speaker placed in the test section to the free-field sound from

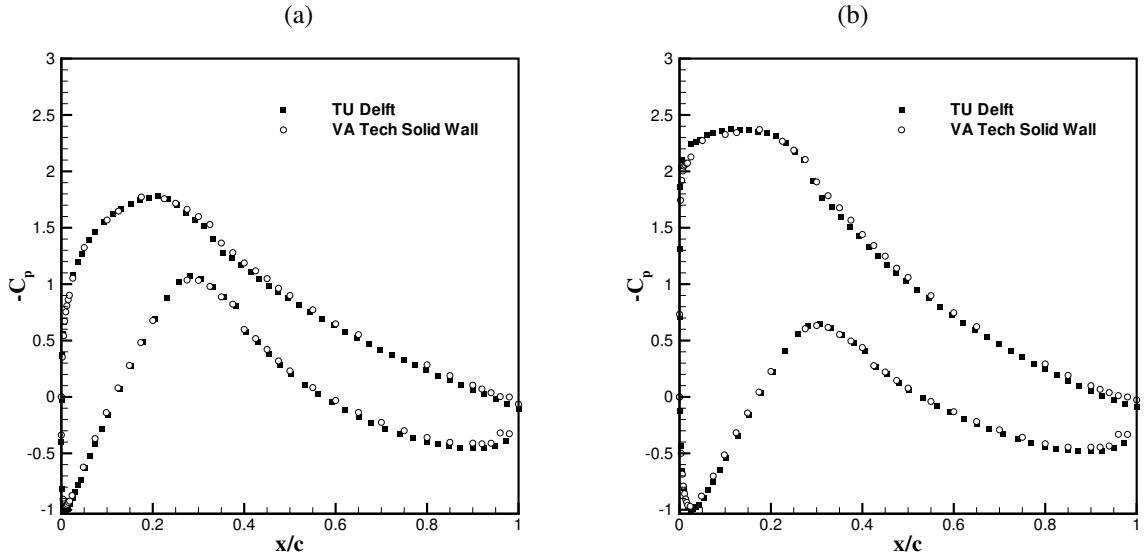

Figure 3. Measured surface pressure coefficient for the DU97-W-300, $\mathbf{Re_c = 3 \times 10^6}$. (a) $\alpha = 4$ deg. (b) $\alpha = 8$ deg.

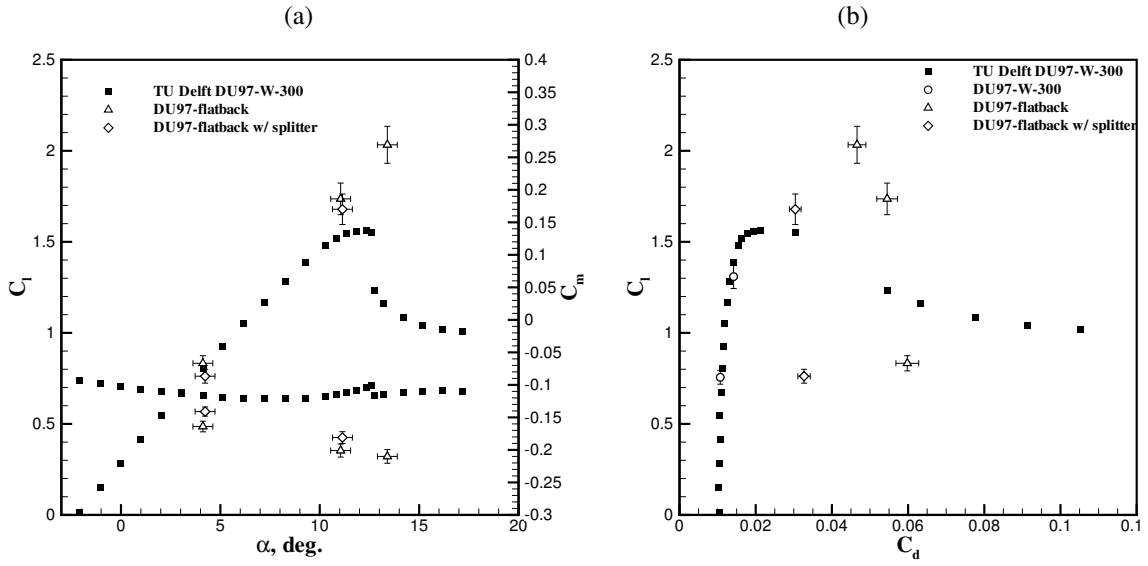

Figure 4. Measured lift, drag and moment coefficient for the DU97-flatback compared with TU Delft DU97-W-300 data, $\mathbf{Re_c = 3 \times 10^6}$.

the same speaker. At the microphone array location and tunnel speed of the present measurements this correction was less than 3 dB above 100 Hz. The attenuation of sound by the tunnel boundary layers at low frequencies was also determined empirically. At a tunnel speed of 50 m/s this correction was 2 dB. Attenuation by the Kevlar material is negligible for frequencies below 5000 Hz.

Averaged (and corrected) acoustic sound pressure level (SPL) spectra at the measurement location for the three configurations at $\alpha = 4$ degrees are presented in Figure 5. The vortex-shedding peak is apparent at 153 Hz for the DU97-flatback with an amplitude of 94 dB. The effect of the splitter plate is to reduce the peak amplitude to 82 dB and shift the frequency of the shedding tone to 188 Hz. The results for $\alpha = 11$ degrees (Figure 6) show the same qualitative behavior, although the peak amplitudes are reduced from the $\alpha = 4$ degree case by about 4 dB. At both angles of attack the splitter plate reduces the peak noise amplitude by 12 dB. Figure 7 shows the effect of tripping the boundary layer on the vortex-shedding sound at $\alpha = 11$ degrees. The boundary layer was tripped using 0.5 mm thick trip tape at $x/c = 0.05$ on the upper surface and at $x/c = 0.10$ on the lower surface. The main effects of tripping on

the flatback noise were to increase its amplitude by 4 dB as well as to narrow the peak. The splitter plate was more effective for the tripped case, reducing the peak SPL by 16.5 dB.

The vortex-shedding noise frequency f_s is best characterized by a non-dimensional Strouhal number, defined by $St \equiv f_s h/U_\infty$, where h is the base height and U_∞ is the free stream velocity. The measured Strouhal number for the tripped and un-tripped DU97-flatback was 0.24 ± 0.01, independent of angle of attack. The presence of the splitter plate increased the Strouhal number to 0.30 ± 0.01 for the untripped cases. For the $\alpha = 10$ degree tripped case with splitter plate, the Strouhal number was 0.27 ± 0.01. This range of Strouhal numbers is in good agreement with previously reported results by Bearman[13] for a blunt trailing edge airfoil with an elliptical leading edge tested at zero angle of attack and at chord Reynolds numbers of 1.45×10^5 and 2.45×10^5.

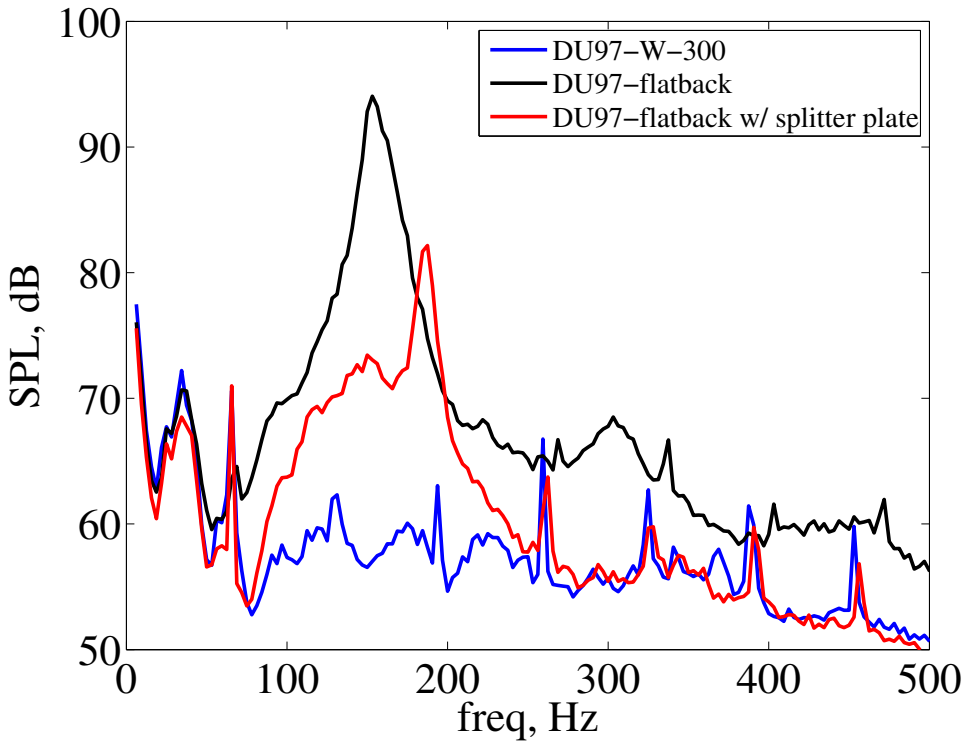

Figure 5. Narrow-band sound pressure level spectra for $\alpha = 4$ degrees.

V. Computational Aerodynamic Predictions

A. Problem Setup and Solution Method

Computational Fluid Dynamics (CFD) results are presented for prediction of aerodynamic force and moment coefficients of the DU97-W-300 and DU97-flatback at a chord Reynolds number of 3×10^6. The CFD predictions were made using the SACCARA code,[14] a structured-grid multi-block finite volume code that solves the compressible Reynolds-averaged Navier-Stokes (RANS) equations using one of several available turbulence models for high-Reynolds number aerodynamics. Predictions were made using both the Spalart-Allmaras one-equation turbulence model[15] and the Menter k-ω model[16] (referred to hereafter as the SA model and the k-ω model, respectively). The numerical scheme used in the SACCARA code was a second order symmetric total-variation-diminishing (STVD) scheme, and all solutions were relaxed to steady state using a point-implicit solver.

The computational grids employed a C-mesh topology, with 800 grid cells along the airfoil surface with clustering near the leading and trailing edges. For the DU97-W-300 grid, 288 grid cells were used in the transverse direction, with a wall-normal grid spacing of 2×10^{-6} m at the airfoil surface and a stretching ratio of 1.06. There were 240 cells across the trailing edge base, which has a height of $0.015c$, and 400 cells in the streamwise direction in the wake. The DU97-flatback grid had the same wall-normal spacing, number of cells across the base height and number of cells along the airfoil surface, but had 248 cells in the transverse direction and 300 streamwise cells in the wake.

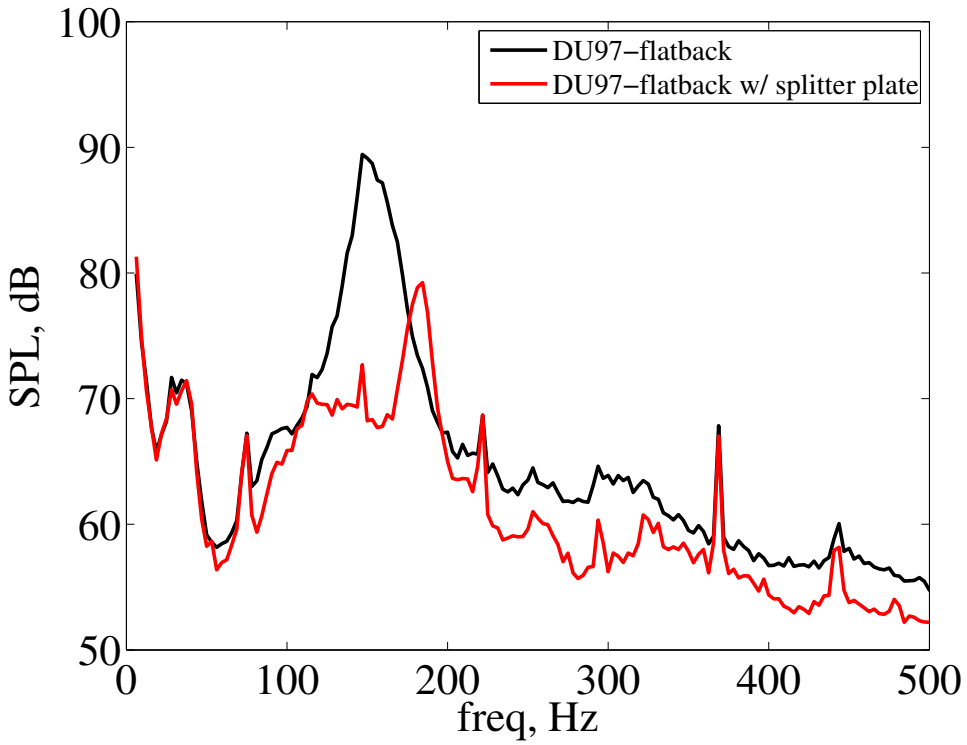

Figure 6. Narrow-band sound pressure level spectra for $\alpha = 11$ degrees, free transition.

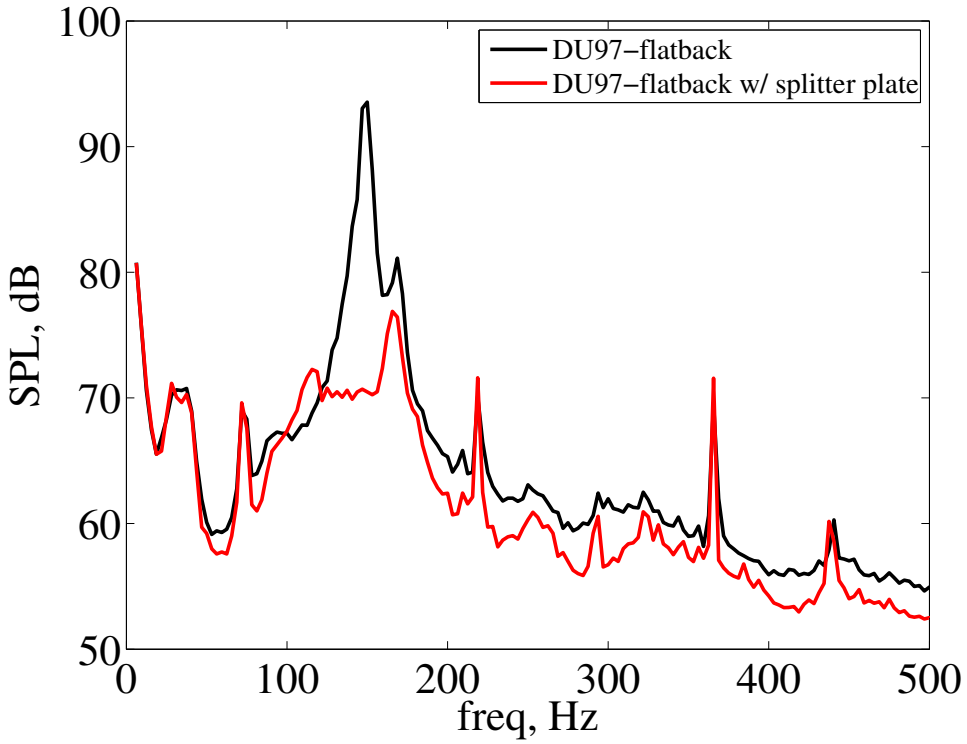

Figure 7. Narrow-band sound pressure level spectrum for $\alpha = 11$ degrees and with boundary layer trip strips applied.

Mesh sensitivity of the solutions was determined to be minimal for these relatively fine grids. In order to obtain grid-converged drag results, sufficient resolution in the near-wake region was required for both airfoils. The maximum value for $y+$ for the first grid cell off the airfoil surface was less than 0.35 for the DU97-W-300 solutions using either turbulence model at $\alpha = 8$ degrees.

An adiabatic no-slip wall boundary condition was applied on the airfoil surface. The total pressure, temperature, and flow angle were held constant at the far-field inflow boundary which was placed $50c$ from the airfoil. At the outflow boundary, also at $50c$, static pressure was held constant. Boundary layer transition locations were predicted for both airfoils using the XFOIL viscous panel method code.[17] These transition locations were then specified in the CFD calculations by explicitly setting the turbulent eddy viscosity to zero upstream of the transition points. The specified transition locations are listed in Table 3. For the flatback with splitter plate computations, the transition locations were the same as those used for the flatback without the splitter plate.

α, deg.	**DU97-W-300 upper surf.**	**DU97-W-300 lower surf.**	**DU97-flatback upper surf.**	**DU97-flatback lower surf.**
0	0.383	0.354	0.361	0.353
2	0.352	0.364	0.338	0.362
4	0.331	0.376	0.318	0.372
6	0.308	0.388	0.298	0.384
8	0.285	0.401	0.264	0.397
10	0.220	0.416	0.161	0.414
12	0.125	0.431	0.065	0.431
14	0.070	0.446	0.033	0.452

Table 3. Specified boundary layer transition locations (x/c) for the CFD calculations.

B. Computational Results

Lift and moment coefficient predictions for the DU97-W-300 are shown in Figure 8. The SA and k-ω model results give comparable agreement with experiment in the linear lift regime. The SA model appears to give a more accurate value for maximum lift coefficient, while the k-ω model lift overshoots the value at stall by a large margin. The SA model gives superior agreement with the experimental moment coefficient data.

Figure 9 compares the computed drag coefficient with the experimental data. The k-ω model, while overpredicting the drag coefficient by approximately 20% in the linear lift region, gives much better results than the SA model. This can largely be attributed to differences in the viscous drag. Figure 10 shows the skin friction coefficient distribution for $\alpha = 8$ degrees for both models. The skin friction for the SA model rises to a much higher level immediately following the transition point on both the upper and lower surfaces. It seems likely that much of this difference between the two models is due to differences in approximating transitional boundary layer behavior, for which neither model is well-suited since transition modeling is not explicitly part of the model formulation.

Surface pressure coefficient distributions are assessed against data from the TU-Delft tunnel in Figures 11 – 13. Agreement for the k-ω model is better at $\alpha = 4$ and $\alpha = 8$ degrees, particularly over the suction surface. However, the $\alpha = 12$ degree data shows a region of separated flow near the trailing edge which is captured by the SA model but not by the k-ω model. This is the specific modeling error that leads to overprediction of the lift near stall for the k-ω model (see Figure 8).

Figure 14 shows the CFD predictions of lift and moment for the DU97-flatback and comparison with the experimental data. Both turbulence models give very similar results, and both agree reasonably well with the data. Interestingly, there is closer agreement between the two turbulence models for the DU97-flatback than for the DU97-W-300. Figure 15 shows the drag predictions for the DU97-flatback. Underprediction of the drag for bluff bodies is a known deficiency of many RANS turbulence models, so the disagreement with experiment is not surprising. The SA model results are closer to the data but still underpredict the drag by as much as 35%. Also, the computations show a conventional drag polar shape while the data show a decrease in drag at higher lift. The experimental pressures near the airfoil base increased as angle of attack increased, leading to this trend, which the computations are unable to reproduce. Unsteady CFD methods that more accurately capture the vortex dynamics of the blunt trailing edge wake, such as Large Eddy Simulation (LES), offer hope of improved prediction of flatback drag.

Figure 16 gives results for the SA model for the DU97-flatback with splitter plate attachment. The k-ω model

computations produced non-physical solutions in the vicinity of the splitter plate, possibly due to insufficient near-wall grid resolution over the splitter plate itself. The k-ω results require further study and so are not presented for the splitter plate case. Lift and moment predictions in Figure 16 show similar good agreement as demonstrated for the DU97-flatback without splitter plate. The agreement for drag has improved, but this must be viewed as coincidental. The decrease in experimental drag offered by the splitter plate is nearly 50%, while a much more modest decrease is predicted by the model.

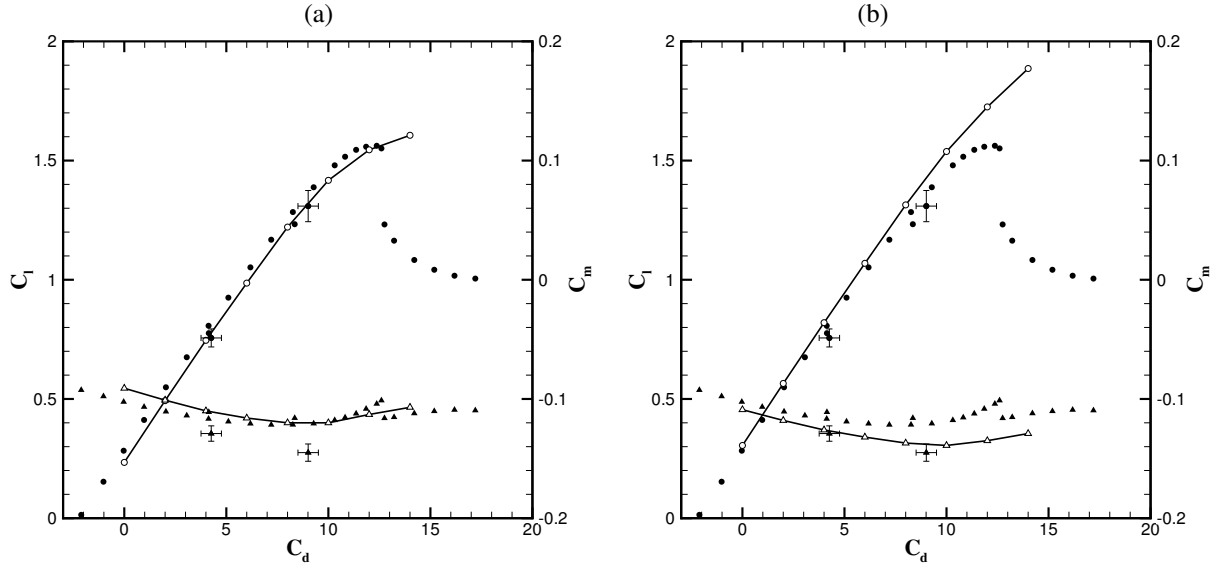

Figure 8. Lift and moment coefficient for the DU97-W-300. (a) Spalart-Allmaras model. (b) k-ω model. Symbols are TU Delft wind tunnel data and lines are CFD results.

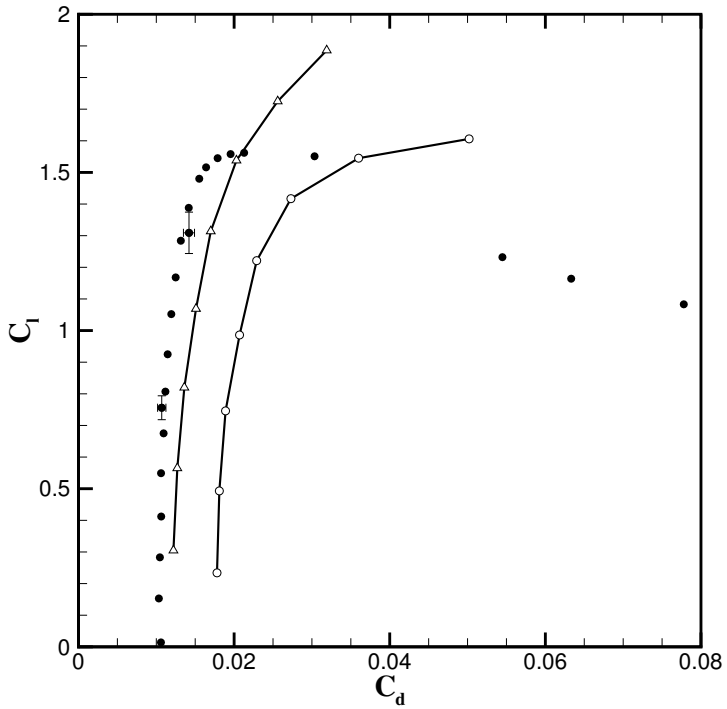

Figure 9. Drag polar for the DU97-W-300. Closed symbols are wind tunnel data and open symbols/lines are CFD results; ◯ : SA model, △ : k-ω model.

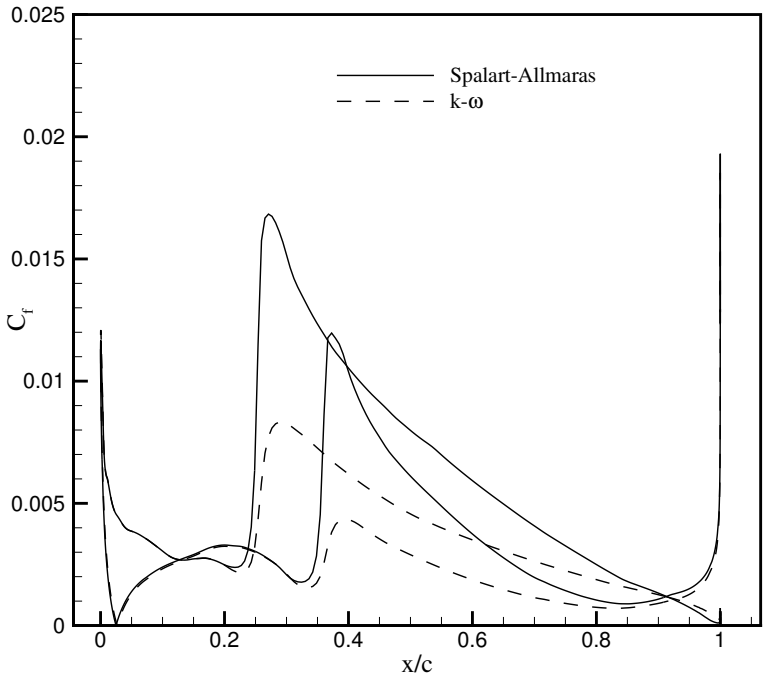

Figure 10. Computed skin friction coefficient for the DU97-W-300.

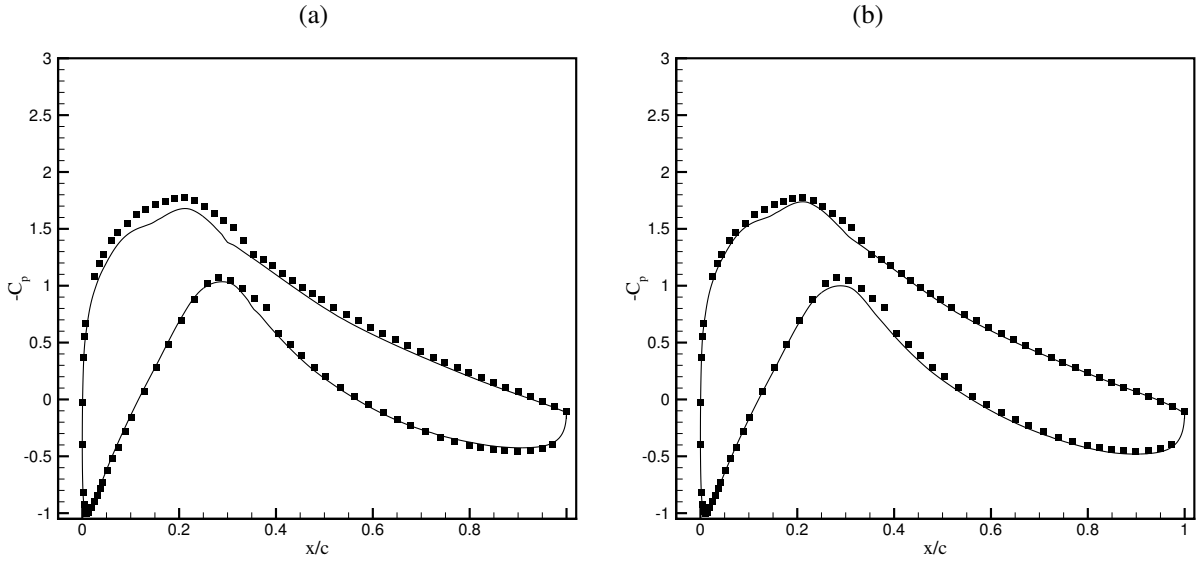

Figure 11. Surface pressure coefficient for the DU97-W-300, $\alpha = 4$ degrees. (a) Spalart-Allmaras model. (b) k-ω model. Closed symbols are wind tunnel data and open symbols/lines are CFD results.

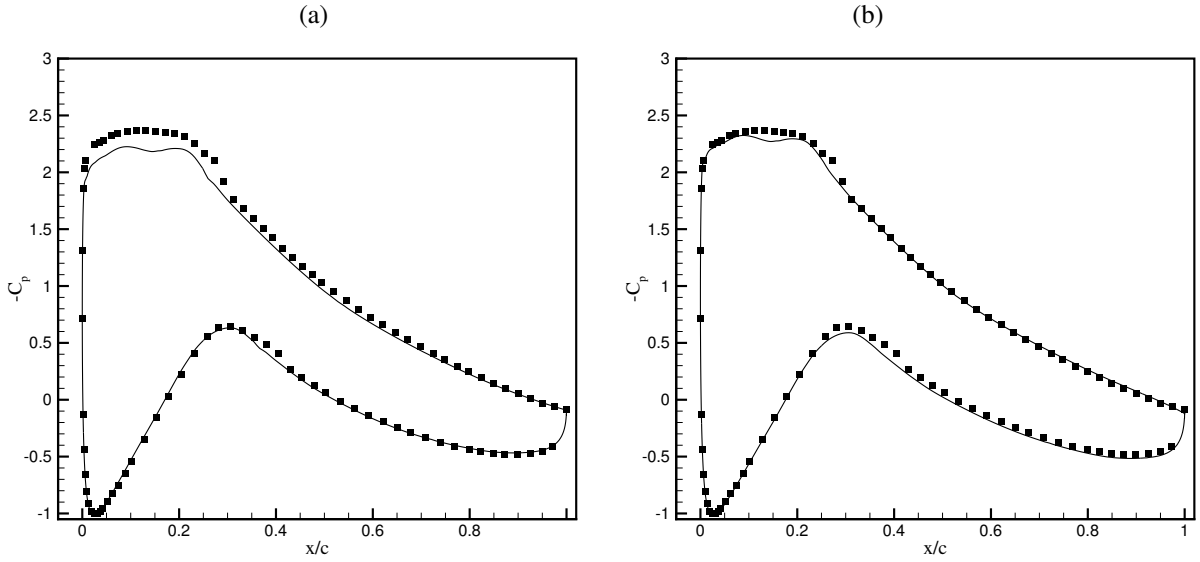

Figure 12. Surface pressure coefficient for the DU97-W-300, $\alpha = 8$ degrees. (a) Spalart-Allmaras model. (b) k-ω model. Closed symbols are wind tunnel data and open symbols/lines are CFD results.

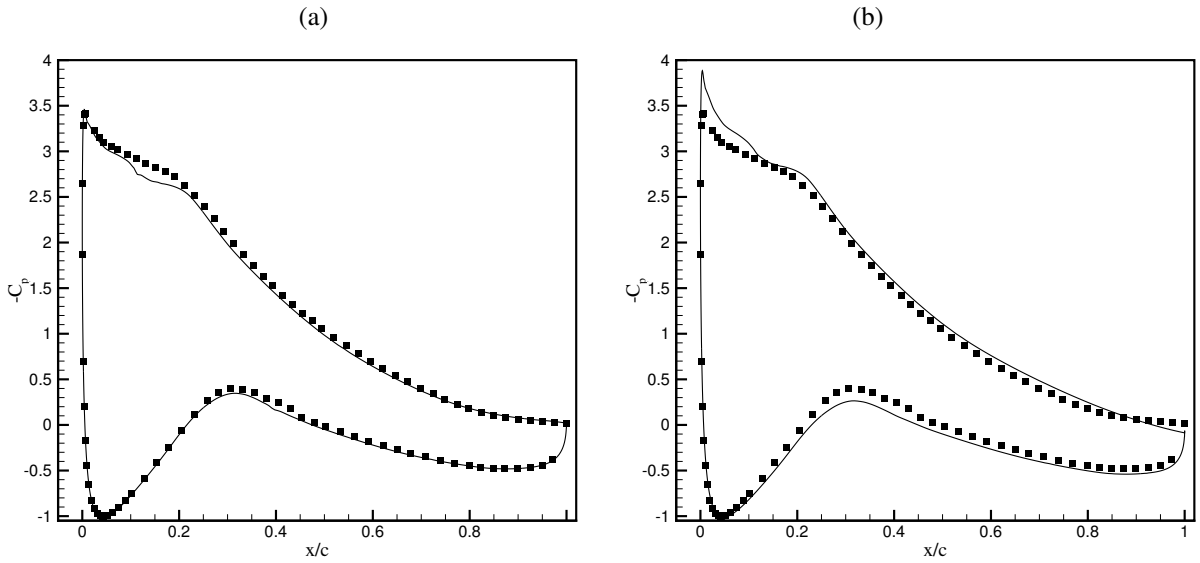

Figure 13. Surface pressure coefficient for the DU97-W-300, $\alpha = 12$ degrees. (a) Spalart-Allmaras model. (b) k-ω model. Closed symbols are wind tunnel data and open symbols/lines are CFD results.

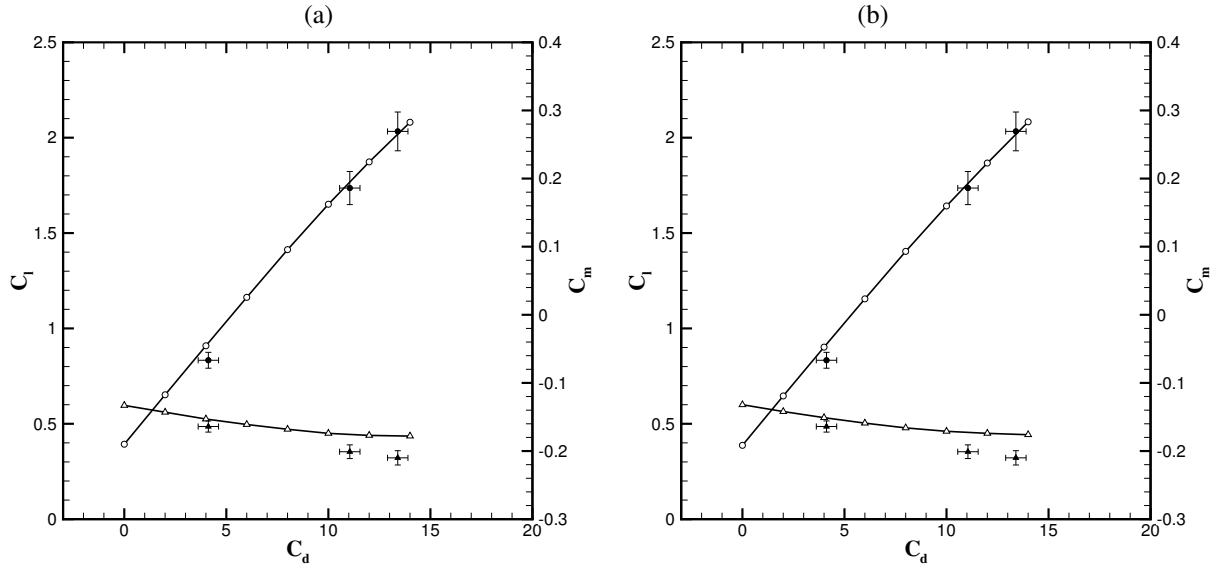

Figure 14. Lift and moment coefficient for the DU97-flatback. (a) Spalart-Allmaras model. (b) k-ω model. Closed symbols are wind tunnel data and open symbols/lines are CFD results.

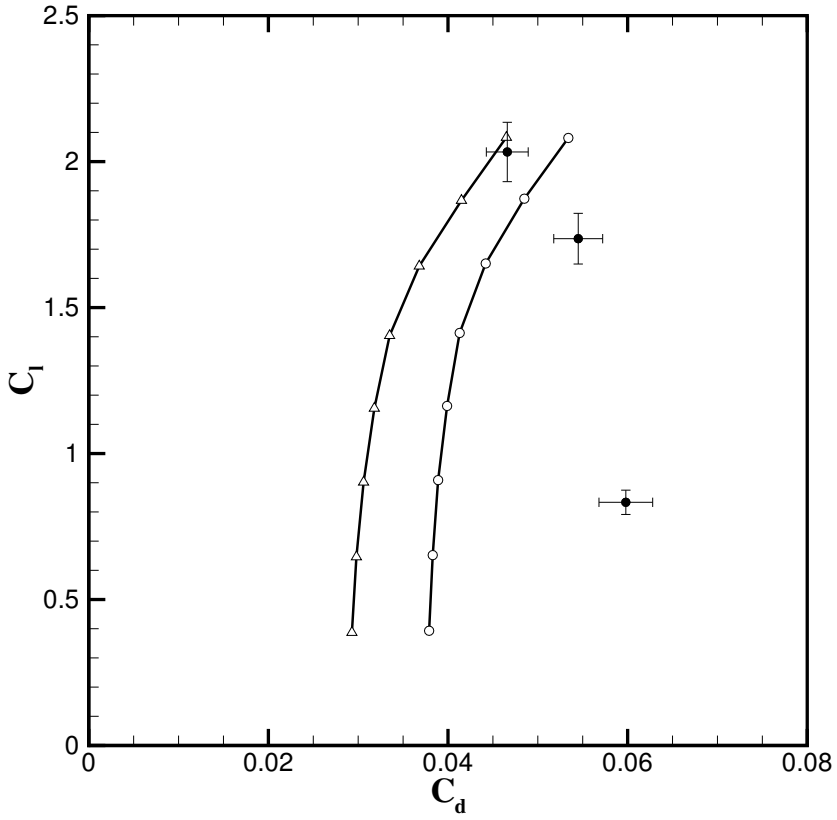

Figure 15. Drag polar for the DU97-flatback. Closed symbols are wind tunnel data and open symbols/lines are CFD results; ◯ : SA model, △ : k-ω model.

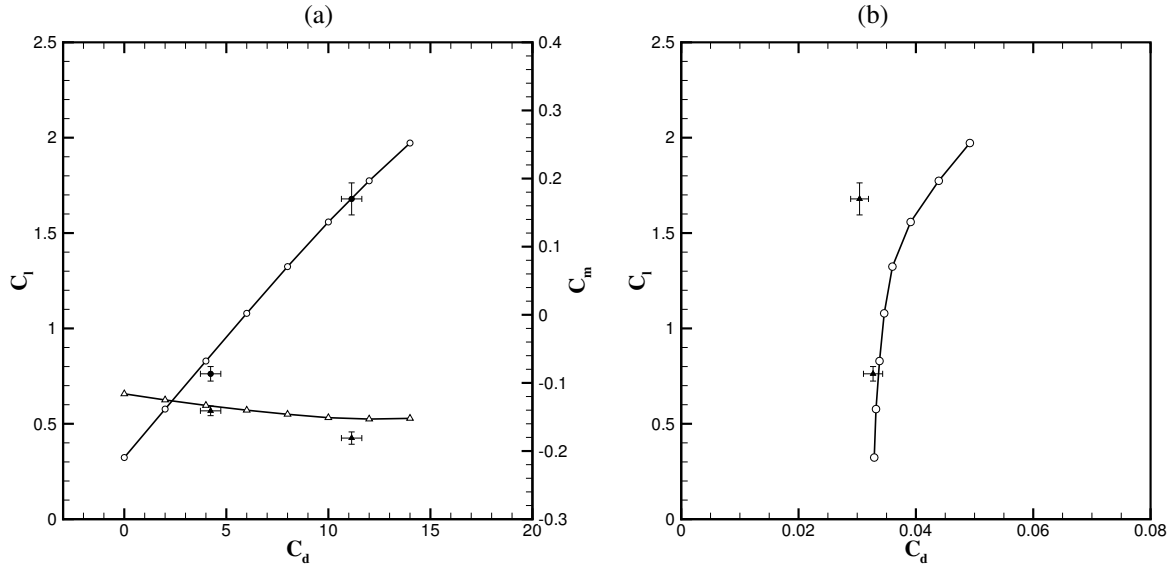

Figure 16. SA model predictions for the DU97-flatback with spliiter plate. (a) Lift and moment coefficient. (b) Drag polar. Closed symbols are wind tunnel data and open symbols/lines are CFD results.

VI. Conclusions

Experimental and computational results have been presented for the DU97-W-300 airfoil and a flatback version of that airfoil, operating at a chord Reynolds number of 3 million. The increase in lift curve slope and maximium lift coefficient that has been reported at lower Reynolds numbers is also observed at this higher Reynolds number. Drag penalties are severe, as expected, but the drag can be reduced by up to 50% using a simple splitter plate attachment, in accord with results at lower Reynolds number. CFD predictions of the lift for the DU97-W-300 and the DU97-flatback are in good agreement with the experimental data, except for near stall where proper prediction of the onset of trailing edge separation by the turbulence model is crucial. Agreement of the computations with experimental pitching moment is decent, while drag is overpredicted for the DU97-W-300 and underpredicted for the DU97-flatback.

Acoustic measurements verify the presence of a distinct vortex-shedding tone at a Strouhal number of 0.24 for the flatback airfoil. The splitter plate attachment reduces the amplitude of this tone by 12 dB and shifts the Strouhal number to 0.30. Increasing the angle of attack from four to eleven degrees reduced the peak SPL by about 4 dB for the flatback with and without the splitter plate. The present aeroacoustic measurements provide a basis for constructing and validating simple models of flatback airfoil noise. Further analysis using such models will be required to assess the effect of flatback airfoil noise on the overall noise spectrum of a utility-scale wind turbine rotor.

VII. Acknowledgements

The authors acknowledge the efforts of William Devenport, Ricardo Burdisso, Aurelian Borgoltz, and their assistants at Virginia Tech who performed the wind tunnel tests. The authors also gratefully acknowledge Nando Timmer from TU Delft for providing wind tunnel data for the DU97-W-300. This work was funded through Sandia National Laboratories by the Department of Energy's Wind and Hydropower Technologies Program. Sandia is a multiprogram laboratory operated by Sandia Corporation, a Lockheed Martin Company for the United States Department of Energy's National Nuclear Security Administration under contract DE-AC04-94AL85000.

References

[1]J. A. Paquette and P.S. Veers. Increased strength in wind turbine blades through innovative structural design. *Proceedings of the European Wind Energy Conference*, 2007.

[2]J.P. Baker, E.A. Mayda, and C.P. van Dam. Experimental analysis of thick blunt trailing-edge wind turbine airfoils. *J. Solar Energy Engineering*, 128:422–431, 2006.

[3]K.J. Standish and C.P. van Dam. Aerodynamic analysis of blunt trailing edge airfoils. *J. Solar Energy Engineering*, 125:479–487, 2003.

[4]D.D. Chao and C.P. van Dam. Computational aerodynamics analysis of a blunt trailing-edge airfoil modification to the NREL phase VI rotor. *Wind Energy*, 10(6):529–550, 2007.

[5]W.A. Timmer and R.P.J.O.M. van Rooij. Summary of the Delft University wind turbine dedicated airfoils. *J. Solar Energy Engineering*, 125:488–496, 2003.

[6]D. E. Berg and J. R. Zayas. Aerodynamic and aeroacoustic properties of flatback airfoils. AIAA Paper 2008-1455, 2008.

[7]C. Stone, M.F. Barone, M.J. Smith, and C.E. Lynch. A computational study of the aerodynamics and aeroacoustics of a flatback airfoil using hybrid RANS-LES. AIAA Paper 2009-0273, 2009.

[8]M. Remillieux, E. Crede, H. Camargo, R. Burdisso, W. Devenport, M. Rasnick, P. van Seeters, and A. Chou. Calibration and demonstration of the new Virginia Tech anechoic wind tunnel. AIAA 2008-2911, 2008.

[9]H.J. Allen and W.G. Vincenti. Wall interference in a two-dimensional-flow wind tunnel, with consideration of the effect of compressibility. NACA Report No. 782, 1947.

[10]B.F.R. Ewald. Wind tunnel wall correction. AGARD-AG-336, 1998.

[11]C.P. van Dam, E.A. Mayda, and D.D. Chao. Computational design and analysis of flatback airfoil wind tunnel experiment. Technical Report SAND2008-1782, Sandia National Laboratories, 2008.

[12]J.P. Baker, C.P. van Dam, and B.L. Gilbert. Flatback airfoil wind tunnel experiment. Technical Report SAND2008-2008, Sandia National Laboratories, 2008.

[13]P.W. Bearman. Investigation of the flow behind a two-dimensional model with a blunt trailing edge and fitted with splitter plates. *J. Fluid Mech.*, 21:241–255, 1965.

[14]C. C. Wong, F. G. Blottner, J. L. Payne, and M. Soetrisno. Implementation of a parallel algorithm for thermo-chemical nonequilibrium flow solutions. AIAA Paper 95-0152, January 1995.

[15]P. R. Spalart and S. R. Allmaras. A one-equation turbulence model for aerodynamic flows. *Le Recherche Aérospatiale*, 1:5–21, 1994.

[16]F. R. Menter. Improved two-equation k-ω turbulence models for aerodynamic flows. NASA TM-103975, October 1992.

[17]M. Drela and M.B. Giles. Viscous-inviscid analysis of transonic and low-Reynolds number airfoils. *AIAA J.*, 25(10):1347–11355, 1987.